

Supporting information

Mechanisms of iron and copper-frataxin interactions

Thi Hong Lien Han¹, Jean-Michel Camadro², Renata Santos^{2a}, Jean-Michel El Hage Chahine¹, Nguyet-Thanh Ha-Duong^{1*}

* thanh.haduong@univ-paris-diderot.fr

¹ Univ Paris Diderot, Sorbonne Paris Cité, Interfaces, Traitements, Organisation et Dynamique des Systèmes (ITODYS), UMR 7086, CNRS, 15 rue Jean Antoine de Baïf, F-75205 Paris Cedex 13, France; telephone: 33-11-57-27-72-39; fax: 33-11-57-27-72-63

² "Mitochondries, Métaux et Stress Oxydant", Institut Jacques Monod, UMR7592 CNRS-Université Paris Diderot, Sorbonne Paris Cité, 15 rue Hélène Brion, 75205 Paris Cedex 13, France.

2a: present address: Institut de Biologie de l'Ecole Normale Supérieure, rue d'Ulm, 75005, Paris, France

1. Identification of Yfh1

a. SDS PAGE & Western blot

The pI value of Yfh1 is 4.13. Therefore, the DEAE column was previously equilibrated with 50 mM HEPES buffer at pH 7.0. The proteins were eluted by a 0.1 M to 1 M linear gradient of NaCl. The fraction eluting at 0.4 M NaCl contained an intense protein band that migrated at 15 kDa. This band was visualized by Western blot with an anti-frataxin antibody (Figure S1a & S1b). It showed a certain amount of impurities and was, therefore, purified further.

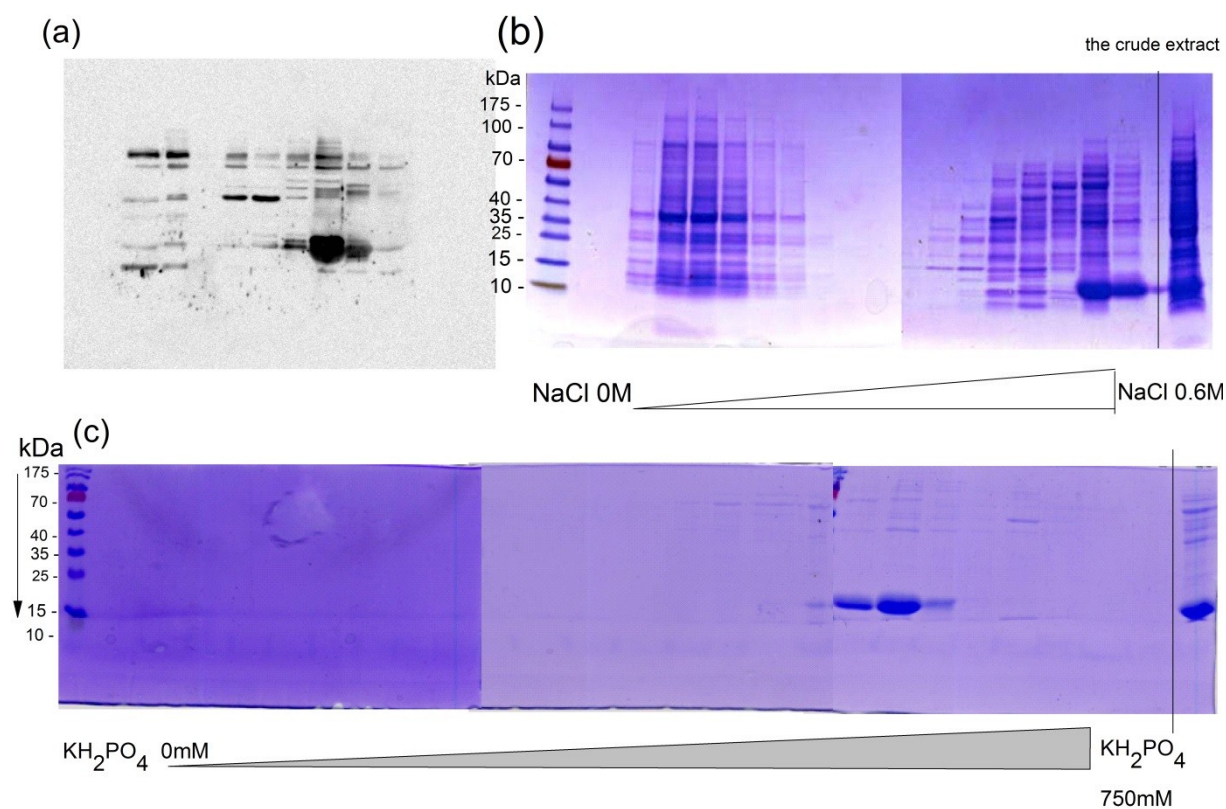


Fig. S1 Protein purification (a) Western blot analysis of fractions eluting from DEAE column; (b) Electrophoresis gel colored by blue coomassie 5% of the fractions eluting from DEAE anion-exchange chromatography column where Yfh1 was eluted at about 0.4 M of NaCl; (c) Electrophoresis gel of the fractions eluting from HAP chromatography where Yfh1 was eluted mainly at 350 mM of KH_2PO_4 .

b. Mass spectroscopy of Yfh1

The purified protein was analyzed by high-resolution electrospray ionization (ESI) mass spectrometry (Orbitrap Exactive EMR). The sample was briefly loaded in a micro-LC column; the elution was monitored by measuring the total ion current. The chromatogram showed a major peak at a retention time of 6.51-6.63 min (Figure S1A). This peak were analyzed and gave a full MS spectrum showing different charged states (Figure S1B). The deconvolution spectrum (Figure S1C) showed a major peak at of 27499.84 Da corresponding to the average mass of a yeast frataxin dimer (theoretical value: 27500.72 Da) with a precision of 0.003 %.

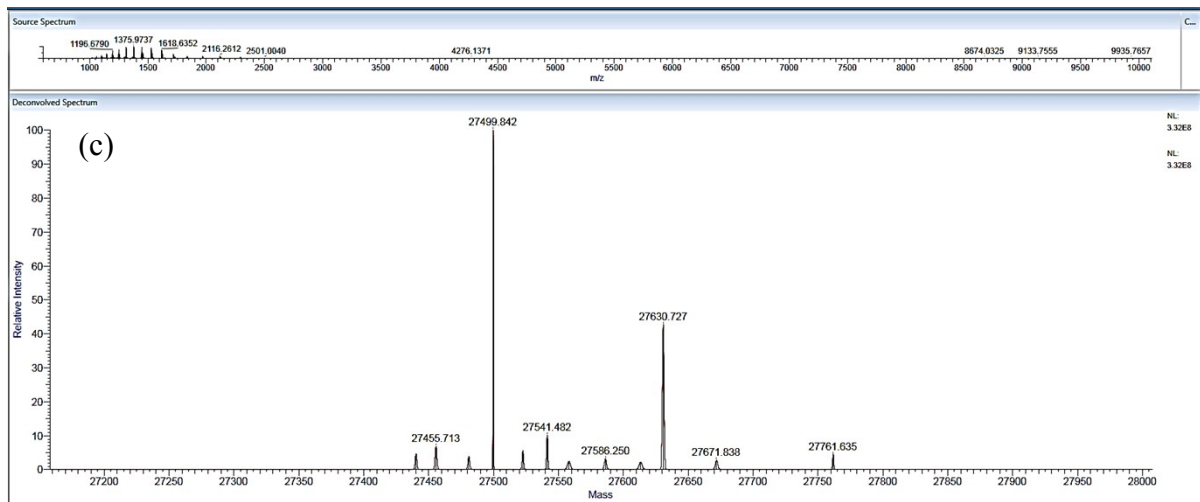
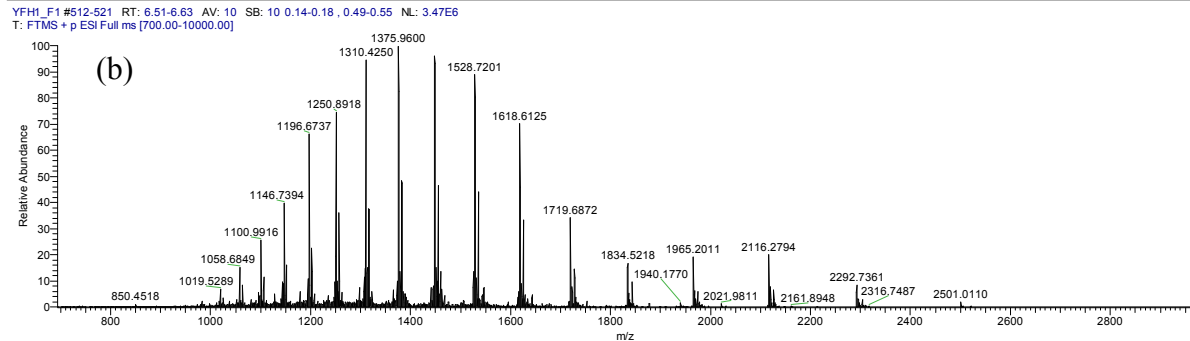
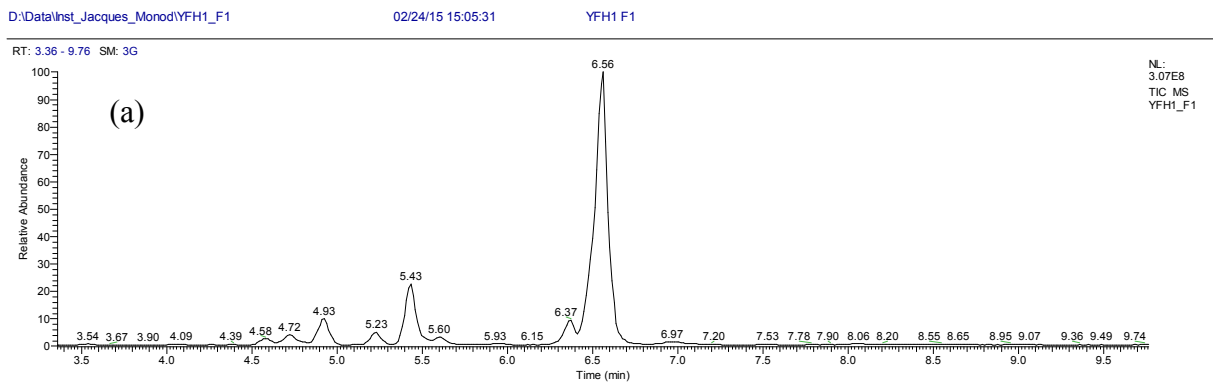
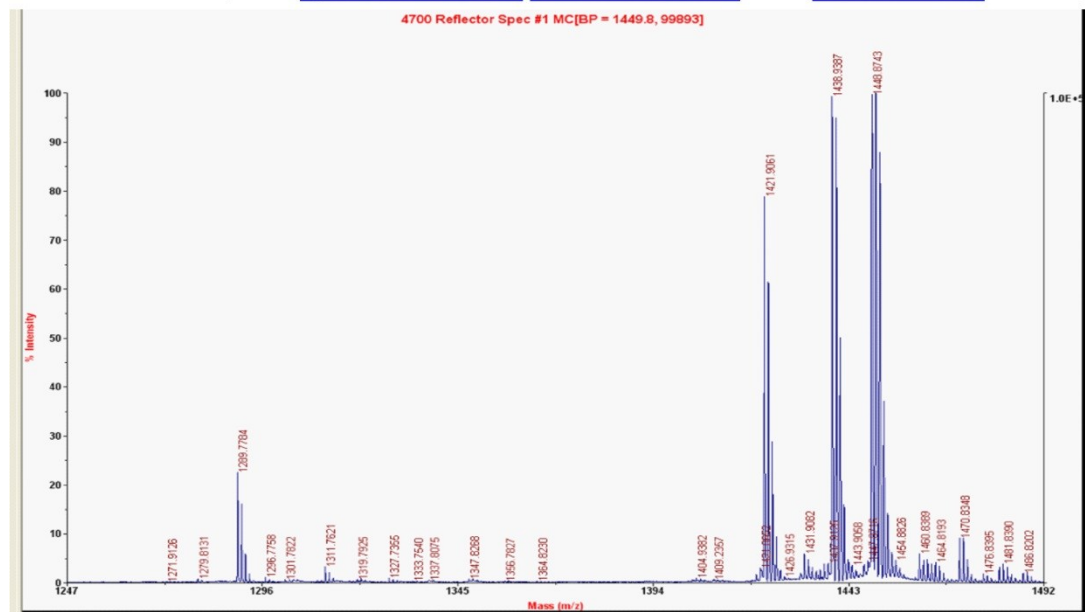


Fig. S2 MS spectra of pure fraction detected by the Exactive Plus EMR MS: (a) Total ion current of flow eluted from micro-LC column (Proswift RP-4H 1x250mm). Elution by a gradient of acetonitrile 0.01 % formic acid from 10 – 80 % in 10 min, flow rate 0.2 mL/min, at 60 °C. The major peak with retention time (RT) is 6.51- 6.63 min was analyzed; (b) ESI full MS spectra with different charge states; (c): Deconvolution spectra confirms the dimeric form of the purified protein. Peak of 27499.842 Da corresponds to theoretical average mass the mature sequence of (yfh1)₂ (27500.72 Da). The 27630.727 Da peak is probably the heterodimer of a full yfh1 with a methionylated yfh1.

c. Peptide mass fingerprint of Yfh1:

We used the peptide mass fingerprint analysis to confirm the expression of the appropriate protein. Indeed, the 15 kDa band in 1D SDS PAGE gel was extracted by TFA 0.1% and digested by trypsin. Figure S2 represents MS spectrum of digested peptides. The limited range of detectable masses for this experiment is 600-3000 Da. MS/MS analysis by MALDI TOF TOF of each fragment allowed exploiting the sequence of each digested peptide (Table S2). The blue peptides in the sequence correspond to the calculate peptides.

MVESSTDGQVVPQEVLNPLEKYH[▼]EEAD[▼]YLDHLLDSLEELSEAH[▼]PD[▼]CIPDVELSHG[▼]VMTL
 EIPAFGTYVINK[▼]QPPN[▼]K[▼]QIWLASPLSGPNR[▼]FDLLNGEWVSLR[▼]NGTK[▼]LTDILTEEVEK[▼]AKISKQ



(*) ▼: cut sites of Trypsin

(b) List of peptide information

Calculate mass	Observed mass	± Da	± ppm	Seq.	Peptide	Modification
1289.6835	1289.7599	0.0764	59	158-168	LTDILTEEVEK	
1438.7802	1421.9061	0.0336	23	129-141	QIWLASPLSGPNR	pyroglutamylation
1438.7802	1438.9204	0.1402	97	129-141	QIWLASPLSGPNR	
1448.7533	1448.8555	0.1022	71	142-153	FDLLNGEWVSLR	

Fig. S3 Peptide fingerprint analysis of cut band from 1D SDS PAGE gel. (a) MS spectrum of digested peptide, the mass of peptides detected in the spectrum is that of the expected sequences (blue). (b) In Table are listed the sequences identified by the MS/MS technique; data from MALDI TOF-TOF were exploited by Mascot.

d. Size exclusion gel chromatography

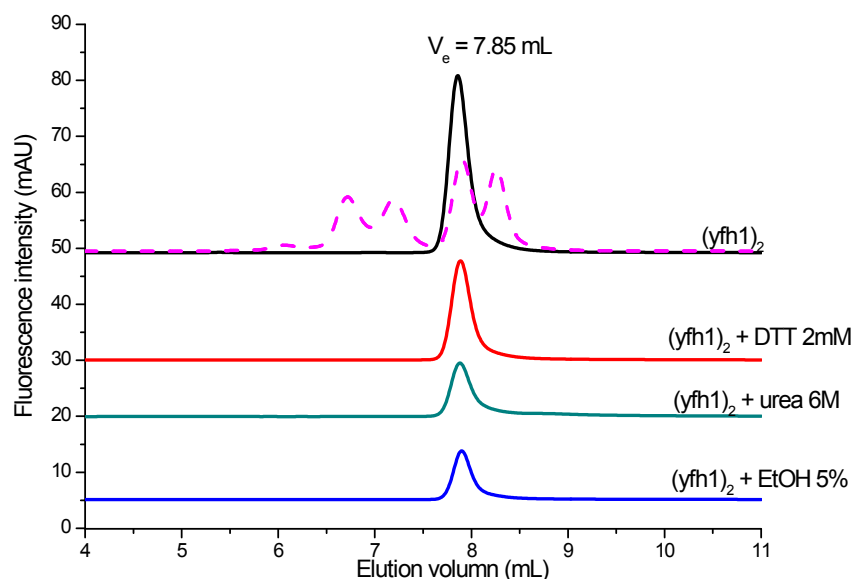


Fig. S4 Size-exclusion chromatography analysis of pure fraction $(Yfh1)_2$ ($V_e = 7.85$ mL) in buffer BisTris 50mM/pH 7.0/ $\mu=0.2$ (black), the same buffer with 2mM DTT (red), urea 6M (green), Ethanol 5% (blue). Mobile phase: KH_2PO_4 50 mM buffer, pH 7.0, injection and elution rate 1 mL/min. Detection by emission spectroscopy $\lambda_{exc} = 280$ nm, $\lambda_{em} = 340$ nm. Overlaid rose line is the chromatogram of calibration mixture containing: dimeric bovine albumin (132 kDa), monomeric bovine albumin (66 kDa), ovalbumin (45 kDa), carbonic anhydrase (29 kDa), lactalbumine (14.2 kDa).

2. Thermodynamic of Frataxin-metal interaction

Iron(III) binding

Iron(III) binding to $(Yfh1)_2$ is investigated in Bis-Tris 50 mM, KCl 150 mM, pH 7.0 by emission spectrophotometry, microcalorimetry and size-exclusion chromatography. The addition of FeNTA to a solution of $(Yfh1)_2$ leads to changes in the emission spectra (Figure S5) as well as to a typical thermogram (Figure S6). The ITC results imply that the binding of Fe^{3+} to $(Yfh1)_2$ is an exothermic process ($\Delta H = -32 \pm 4 \text{ kJ.mol}^{-1}$). The data are curve-fitted by a model of one set of independent binding sites. The fitting yields 9 ± 1 equivalent Fe(III) bound to $(Yfh1)_2$ and a $K_a = 4.0 \times 10^4 \text{ M}^{-1}$

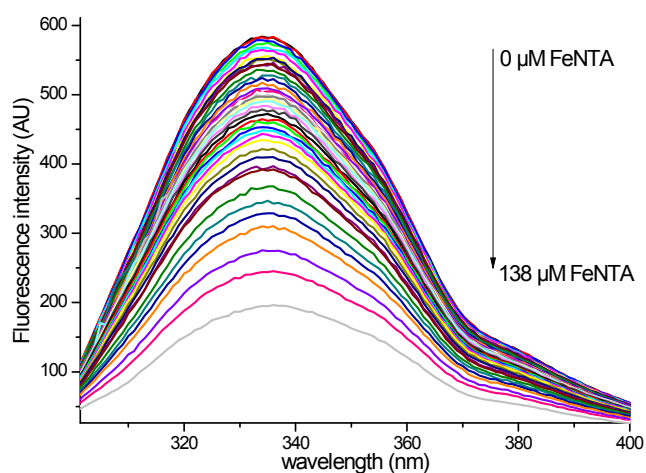


Fig. S5 Emission spectra ($\lambda_{ex} = 280 \text{ nm}$) of $(Yfh1)_2$ ($0.9 \mu\text{M}$) at different concentrations of FeNTA ($0 \mu\text{M}$ to $138 \mu\text{M}$), in 50 mM Bis-Tris, 150 mM KCl, pH 7.0.

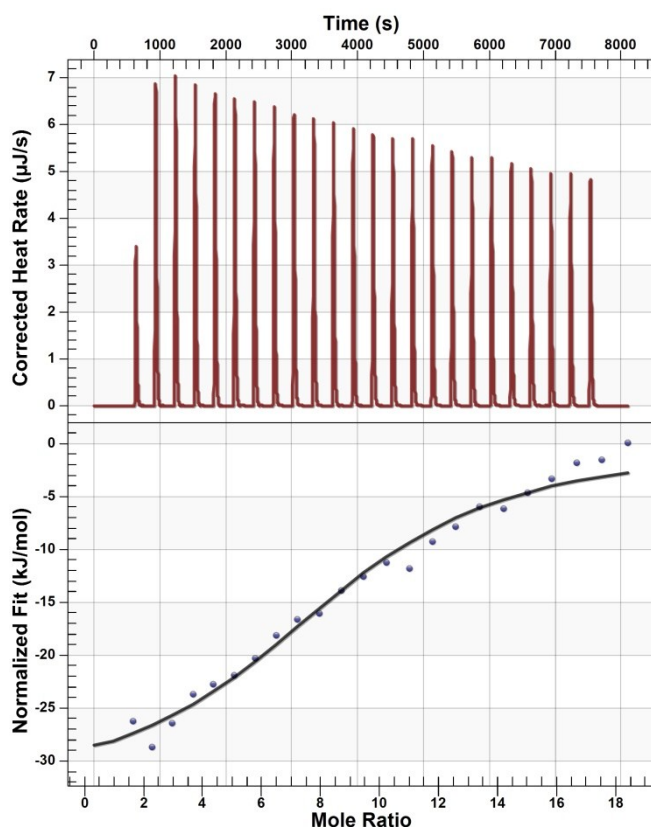


Fig. S6 Raw ITC (top) and binding isotherm data (bottom) for FeNTA to yeast frataxin. The black line in the bottom graph shows the simulated fit to the binding isotherm data. Data were collected at 25°C, pH 7.0, ionic strength $\mu = 0.2$ (Bis-Tris 50 mM, KCl 150 mM).

The solution was afterward injected in a size-exclusion chromatography column. With FeNTA, the absorption and emission chromatograms of the elution profile show two peaks: the first is that of $(Yfh1)_2$ (~28 kDa), whereas, the second is detected at $\sim 60 \pm 5$ kDa. This implies that the presence of Fe^{3+} induces the formation of a stable four frataxin subunits complex (eq. S0, Figure S7).



$$\text{With } K_{\text{dim}} = \frac{[(Yfh1)_4Fe^{III}_{18}]}{[(Yfh1)_2Fe^{III}_9]^2}$$

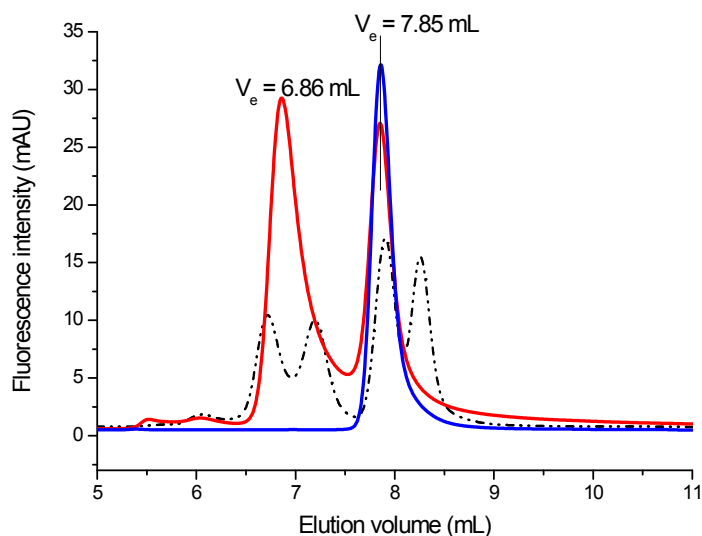


Fig. S7 Chromatograms of $(Yfh1)_2$ ($V_e = 7.85$ mL) in absence (blue) and presence (red) of FeNTA. Mobile phase: 50 mM KH_2PO_4 buffer, pH 7.0, injection and elution rate 1 mL/min. Detection by emission spectroscopy (top) $\lambda_{ex} = 280$ nm, $\lambda_{em} = 340$ nm. Overlaid dash line is the chromatogram of calibration mixture containing: dimeric bovine albumin (132 kDa), monomeric bovine albumin (66 kDa), ovalbumin (45 kDa), carbonic anhydrase (29 kDa), lactalbumine (14.2 kDa).

The dissociation constant of the protein complexes formed between frataxin units in the presence of FeNTA is determined by microcalorimetry. Typically, the complex (2.75 μ M) is injected under stirring into the calorimeter cell (166 μ L) initially containing the buffer, with a typical injection sequence of 25×2 μ l at 5 min intervals. Dilution of the complex in Bis-Tris buffer, pH 7.0, at 25°C gives a series of endothermic heat pulses (Figure S8). This is consistent with the dissociation of protein oligomers modeled as dimers, with a dimerization constant K_{dim} of 2.89×10^5 M^{-1} .

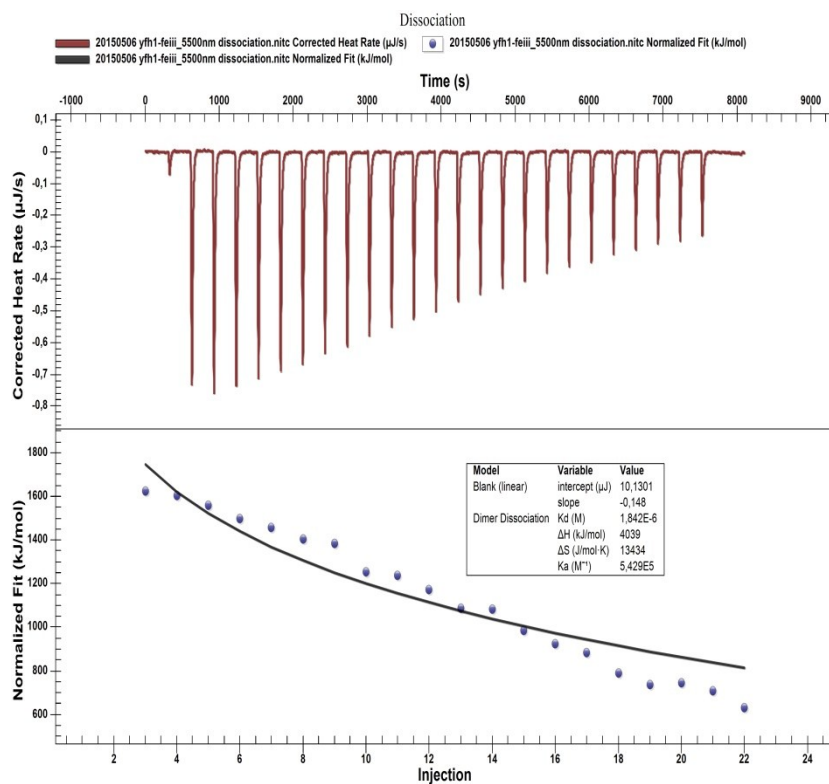


Fig. S8 Raw ITC (top) and dissociation isotherm data (bottom) for $(Yfh1)_4Fe^{III}_{18}$. The black line in the bottom graph shows the simulated fit to the dissociation isotherm data. Data were collected at 25 °C, pH 7.0, ionic strength $\mu = 0.2$ (50 mM Bis-Tris, 150 mM KCl).

Fe(II), Mn(II) and Zn(II) binding

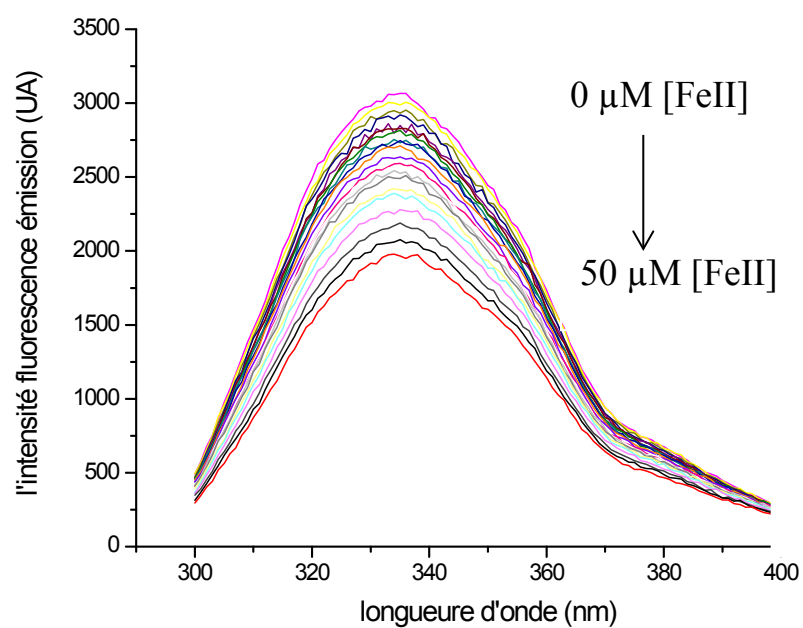


Fig. S9 Variation of the fluorescence intensity of Yfh1 (0.9 μM) at an excitation wavelength $\lambda_{exc} = 280$ nm, in the presence of 2.5 mM GSH

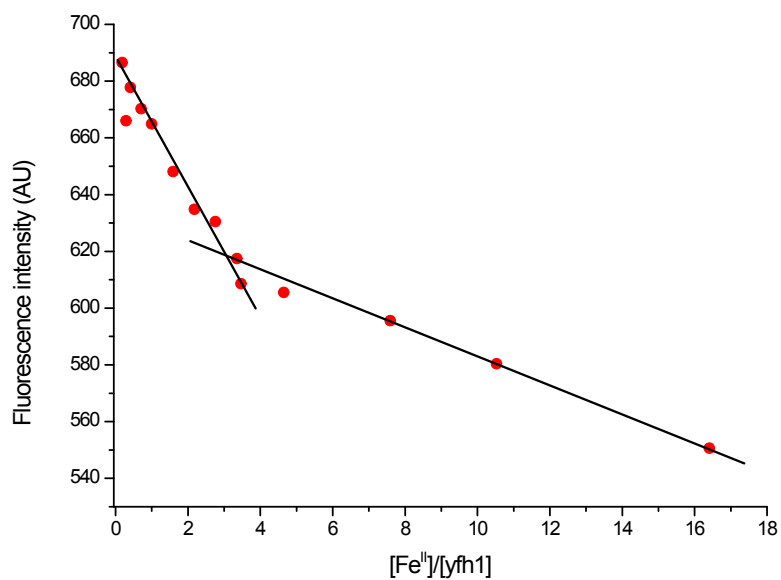


Fig. S10 Fluorescence intensity of Yfh1 at $\lambda_{exc} = 280$ nm, $\lambda_{em} = 334$ nm against [Fe^{II}]/[Yfh1] molar ratios

Yfh1-GSH interaction, size-exclusion chromatography

When two equivalents of GSH are mixed with one equivalent of $(yfh1)_2$, we do not observe any significant change in the elution peak of GSH (Figure S4). This leads us to conclude that there is no interaction between $(Yfh1)_2$ and reduced glutathione.

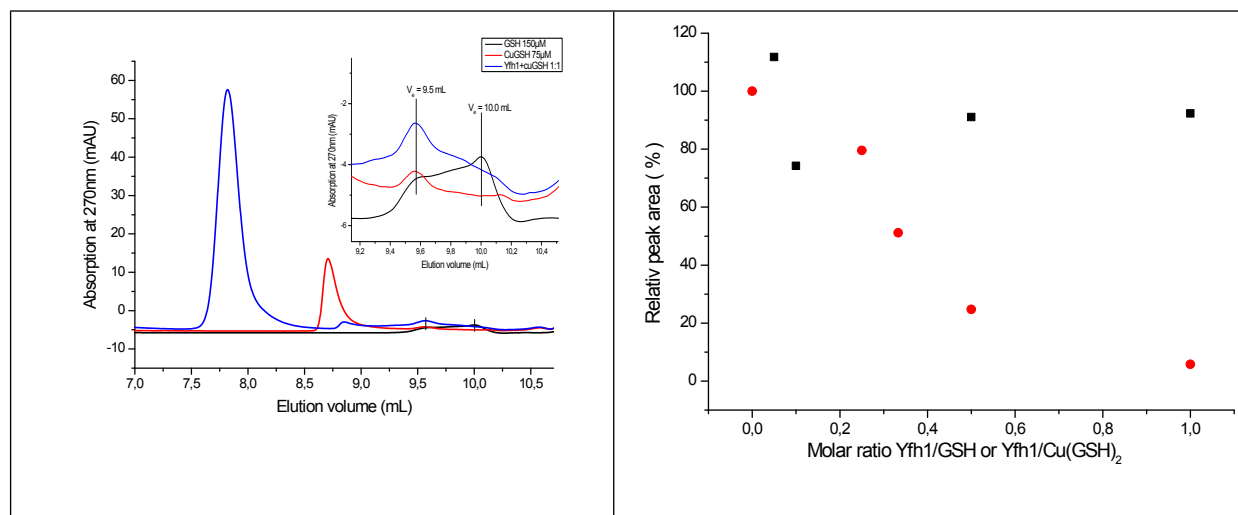


Fig S11 (a) Chromatograms of $\text{Cu}(\text{GSH})_2$ 75 μM in the absence (red), or in the presence of $(yfh1)_2$ 75 μM (blue); GSH 150 μM (black). Inset: zoom-in elution volume corresponding to GSSG/GSH at pH 7.0. Mobile phase: KH_2PO_4 50 mM buffer, pH 7.0, elution rate 1 mL/min. Detection by UV-visible absorbance at $\lambda = 270$ nm. (b) Relative area under curve of GSH peaks (black square) and $\text{Cu}(\text{GSH})_2$ peaks (red circle) in function of molar ratio between Yfh1/GSH or Yfh1/ $\text{Cu}(\text{GSH})_2$.

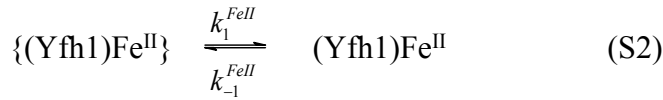
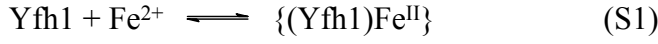
3. Mechanism of Fe(II)-Yfh1 interaction

Kinetics of Iron(II) uptake

When a solution of $(Yfh1)_2$ is rapidly mixed with a solution of Fe^{2+} at pH 7.0, three kinetic processes are observed (Figure S12). The first occurs as an exponential increase in the fluorescence in the 200 ms range (Figure S12A). The second appears as an exponential decrease in fluorescence occurring in about 5 seconds (Figure S12B). These two processes are followed by a third exponential decrease in emission in the 500 s range (Figure S12C). The experimental reciprocal relaxation times related to the first two processes depend on Fe^{2+} concentration, whereas the last process seems independent of all our experimental parameters.

First kinetic process

The experimental reciprocal relaxation times associated with the fast process of Figure S12A depend on Fe^{2+} concentrations in a continuous but non-linear fashion (Figure S13). As already described¹, we ascribe this phenomenon to the fast uptake of a first Fe^{2+} by a frataxin subunit Yfh1 (eq. S1), followed by a rate-limiting monomolecular reaction (eq. S2).



With a dissociation constant $K_1^{FeII} = \frac{[Yfh1][Fe^{2+}]}{[\{(Yfh1)Fe^{II}\}]}$ and $(K_1^{FeII})^{-1} = \frac{[\{(Yfh1)Fe^{II}\}]}{[(Yfh1)Fe^{II}]} = \frac{k_1^{FeII}}{k_{-1}^{FeII}}$

The rate equation of eq. S2 can be expressed as eq. S3:

$$\frac{d\Delta[(yfh1)Fe^{II}]}{dt} = k_1^{FeII} \Delta[\{(yfh1)Fe^{II}\}] - k_{-1}^{FeII} \Delta[(yfh1)Fe^{II}] \quad (S3)$$

Masse conservation allows us to write:

$$\Delta[\{(yfh1)Fe^{II}\}] + \Delta[(yfh1)Fe^{II}] + \Delta yfh1 = 0 \quad (S4)$$

$$\Delta[yfh1] = \frac{K_1^{FeII}}{[Fe^{2+}]} \Delta[\{(yfh1)Fe^{II}\}] \quad (S5)$$

$$\Rightarrow \Delta[\{(yfh1)Fe^{II}\}] = - \left(\frac{[Fe^{2+}]}{K_1^{FeII} + [Fe^{2+}]} \right) \Delta[(yfh1)Fe^{II}] \quad (S6)$$

From Eq. S6 and eq. S3, we derive eq. S7:

$$\frac{d\Delta[(yfh1)Fe^{II}]}{dt} = - \left(k_1^{FeII} \frac{[Fe^{2+}]}{K_1^{FeII} + [Fe^{2+}]} + k_{-1}^{FeII} \right) \Delta[(yfh1)Fe^{II}] \quad (S7)$$

The reciprocal relaxation time equation associated with eq. S2 can be expressed as eq. S8:

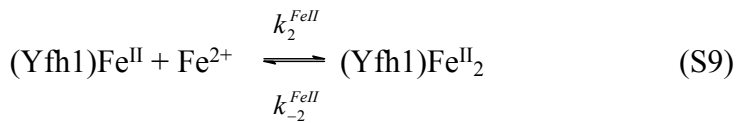
$$(\tau_1^{FeII})^{-1} = k_1^{FeII} \frac{[Fe^{2+}]}{K_1^{FeII} + [Fe^{2+}]} + k_{-1}^{FeII} \quad (S8)$$

Varying K_1^{FeII} from 10 to 1000 μM with a ΔK_1^{FeII} step of 10 μM shows that the best linear regression of $(\tau_1^{FeII})^{-1}$ against $[Fe^{2+}]/(K_1^{FeII} + [Fe^{2+}])$ is obtained for $K_1^{FeII} = 200 \pm 10 \mu M$

(Inset Figure S12). From the slope and intercept, $k_1^{FeII} = 23 \pm 1 \text{ s}^{-1}$, $k_{-1}^{FeII} = 11.5 \pm 0.7 \text{ s}^{-1}$ and $(K_1^{FeII})' = 2.0 \pm 0.1$ are determined.

Second kinetic process

The experimental reciprocal relaxation times associated with this second process depend on $[\text{Fe}^{2+}]$. This phenomenon is assumed to be the uptake of a second Fe^{2+} (eq S9). The reciprocal relaxation time equation associated with this equation is expressed as eq. S10:



$$(\tau_2^{FeII})^{-1} = k_2^{FeII} ([(\text{Yfh1})\text{Fe}^{II}] + [\text{Fe}^{2+}]) + k_{-2}^{FeII} \quad (\text{S10})$$

Since, under our experimental conditions, $[\text{Fe}^{2+}] \gg [(\text{Yfh1})\text{Fe}^{II}]$, eq. S10 simplifies to eq. S11:

$$(\tau_2^{FeII})^{-1} = k_2^{FeII} ([\text{Fe}^{2+}]) + k_{-2}^{FeII} \quad (\text{S11})$$

A very good linear least-squares regression of the experimental $(\tau_2^{FeII})^{-1}$ against $[\text{Fe}^{2+}]$ is obtained (Figure S14). From the slopes and intercepts of the best line, $k_2^{FeII} = (1.15 \pm 0.04) \times 10^3 \text{ M}^{-1} \text{ s}^{-1}$, $k_{-2}^{FeII} = (9.9 \pm 1.3) \times 10^{-2} \text{ s}^{-1}$ and $K_2^{FeII} = k_2^{FeII} / k_{-2}^{FeII} = (1.2 \pm 0.2) \times 10^4 \text{ M}^{-1}$ values are determined.

Third kinetic process

The last kinetic process lasts 500s and seems to be independent of Fe^{2+} concentration.

$$(\tau_3^{FeII})^{-1} = (8 \pm 1) \times 10^{-3} \text{ s}^{-1}.$$

First order kinetics describe monomolecular processes, such as prototropies, ring-chain openings, etc. With proteins these processes are mainly related to changes in conformation (Hémadi, 2004; Eid, 2014). In our case, the relaxation times were independent of the concentrations and the pH, thus leading to a first order kinetic process which implies a conformational change.

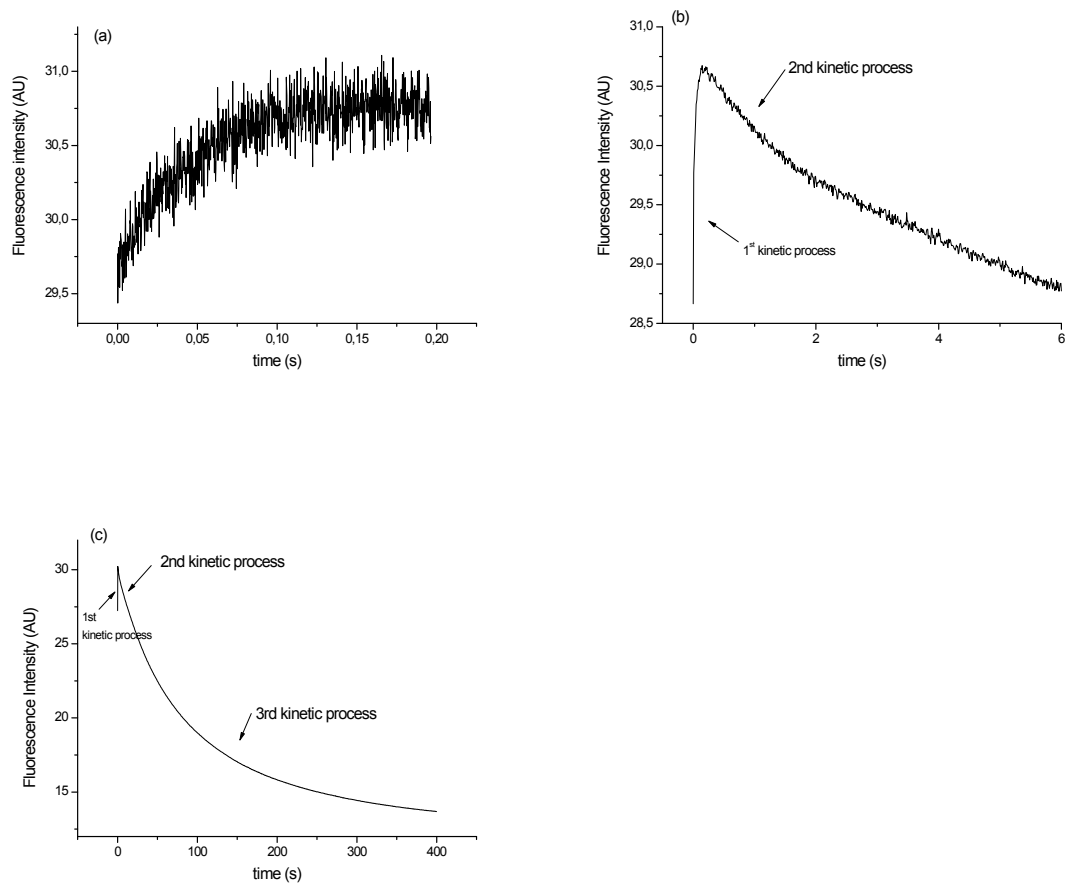


Fig S12 Fluorescence intensity variation with time after a fast mixing of a $(Yfh1)_2$ solution ($0.5 \mu\text{M}$) with a Fe^{2+} solution ($250 \mu\text{M}$) at pH 7.0, $25.0 \text{ }^\circ\text{C}$ and ionic strength $\mu = 0.2$ (50 mM Bis-Tris, 150 mM KCl). (a) recorded over 200 ms (b) recorded over 6 s (c) recorded over 400 s.

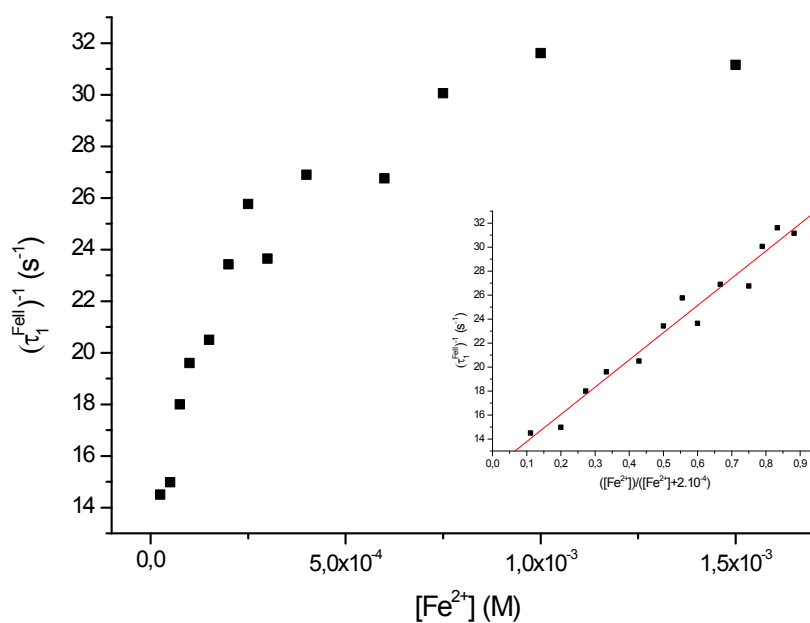


Fig S13 Plot of $(\tau_1^{FeII})^{-1}$ against $[Fe^{2+}]$ at pH 7.0 and 25 °C. Inset: Plot of $(\tau_1^{FeII})^{-1}$ against $[Fe^{2+}]/([Fe^{2+}] + K_1^{FeII})$ with $K_1^{FeII} = 200 \mu\text{M}$; slope, $22.7 \pm 1.2 \text{ s}^{-1}$; intercept, $11.5 \pm 0.7 \text{ s}^{-1}$; $r = 0.98418$.

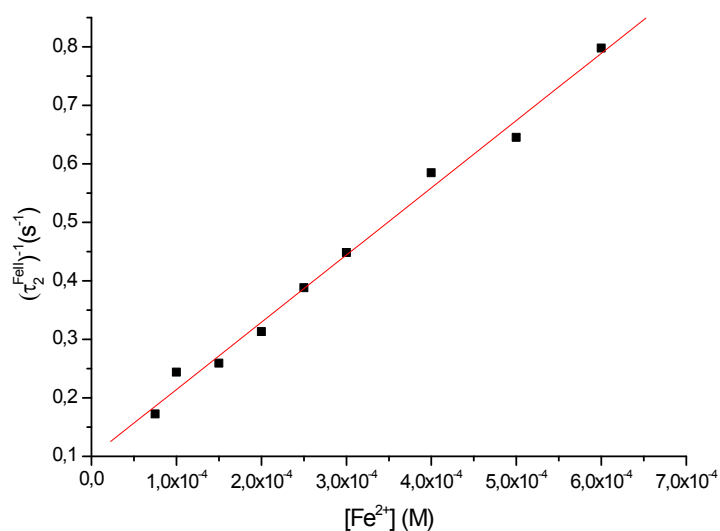
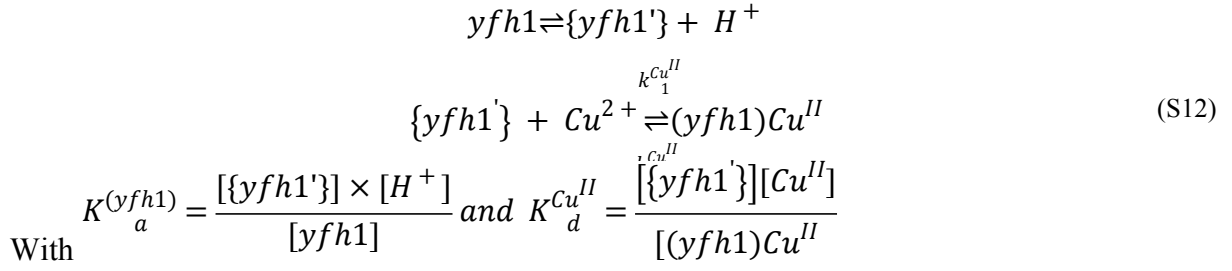


Fig. S14 Plot of $(\tau_2^{FeII})^{-1}$ against $[Fe^{2+}]$ at pH 7.0 and 25 °C; slope, $(1.15 \pm 0.04) \times 10^3 \text{ s}^{-1} \text{ M}^{-1}$; intercept, $(9.9 \pm 1.3) \times 10^{-2} \text{ s}^{-1}$; $r = 0.98947$.

Mechanism of Cu(II)-Yfh1 interaction

a. First kinetic process



The rate equation S12 can be expressed as eq. S13:

$$\frac{d\Delta[(yfh1)Cu^{II}]}{dt} = k_1^{Cu^{II}} \Delta[\{yfh1'\}][Cu^{2+}] - k_{-1}^{Cu^{II}} \Delta[(yfh1)Cu^{II}] \quad (S13)$$

Masse conservation allows to write:

$$\Delta[yfh1] + \Delta[\{yfh1'\}] + \Delta[(yfh1)Cu^{II}] = 0 \quad (S14)$$

As $K_a^{(yfh1)} = \frac{[\{yfh1'\}] \times [H^+]}{[yfh1]}$, we have: $\Delta[yfh1] = \Delta[\{yfh1'\}] \frac{[H^+]}{K_a^{(yfh1)}}$. Eq. S14 becomes eq. S15:

$$\Delta[\{yfh1'\}] \left(1 + \frac{[H^+]}{K_a^{(yfh1)}} \right) = -\Delta[(yfh1)Cu^{II}] \quad (S15)$$

The substitution of eq. S15 in eq. S13 leads to:

$$\frac{d\Delta[(yfh1)Cu^{II}]}{dt} = - \left(k_1^{Cu^{II}} \left(1 + \frac{[H^+]}{K_a^{(yfh1)}} \right)^{-1} [Cu^{2+}] + k_{-1}^{Cu^{II}} \right) \Delta[(yfh1)Cu^{II}] \quad (S16)$$

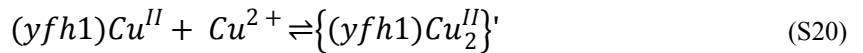
Thus, the reciprocal relaxation time associated with eq. S12 can be expressed as eq. S17:

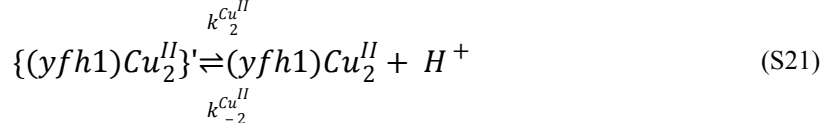
$$(\tau_1^{Cu^{II}})^{-1} = k_1^{Cu^{II}} \times \left(1 + \frac{[H^+]}{K_a^{(yfh1)}} \right) [Cu^{2+}] + k_{-1}^{Cu^{II}} \quad (S17)$$

With: $k_{1obs} = k_1^{Cu^{II}} \left(1 + \frac{[H^+]}{K_a^{(yfh1)}} \right)^{-1}$ (S18)

Or : $\frac{1}{k_{1obs}^{Cu^{II}}} = \frac{1}{k_1^{Cu^{II}}} + \frac{1}{k_1^{Cu^{II}} \cdot K_a^{(yfh1)}} [H^+]$ (S19)

b. Second kinetic process





$$\text{With: } K_{d1} = \frac{[yfh1][Cu^{2+}]}{[(yfh1)Cu^{II}]} ; K_{d2} = \frac{[(yfh1)Cu^{II}][Cu^{2+}]}{[(yfh1)Cu_2^{II}]} \text{ and } K_{a2} = \frac{[\{(yfh1)Cu_2^{II}\}][H^+]}{[(yfh1)Cu_2^{II}]} \quad (S22)$$

$$\Delta[(yfh1)] = K_{d1} \frac{\Delta[(yfh1)Cu^{II}]}{[Cu^{2+}]} = K_{d1}K_{d2} \frac{\Delta[(yfh1)Cu_2^{II}]}{[Cu^{2+}]^2} \quad (S23)$$

$$\Delta[(yfh1)Cu^{II}] = K_{d2} \frac{\Delta[(yfh1)Cu_2^{II}]}{[Cu^{2+}]} \quad (S23)$$

The rate equation of eq. S21 is expressed as eq. S24:

$$\frac{d\Delta[\{(yfh1)Cu_2^{II}\}']}{dt} = k_2^{Cu^{II}} \Delta[(yfh1)Cu_2^{II}] - k_{-2}^{Cu^{II}} [H^+] \Delta[\{(yfh1)Cu_2^{II}\}'] \quad (S24)$$

Mass conservation is expressed as eq. S25 :

$$\Delta[(yfh1)] + \Delta[(yfh1)Cu^{II}] + \Delta[(yfh1)Cu_2^{II}] + \Delta[\{(yfh1)Cu_2^{II}\}'] = 0 \quad (S25)$$

From eq. S24 and S25, we derive eq. S26:

$$K_{d1}K_{d2} \frac{\Delta[(yfh1)Cu_2^{II}]}{[Cu^{2+}]^2} + K_{d2} \frac{\Delta[(yfh1)Cu_2^{II}]}{[Cu^{2+}]} + \Delta[(yfh1)Cu_2^{II}] = -\Delta[\{(yfh1)Cu_2^{II}\}'] \quad (S26)$$

$$\Delta[\{(yfh1)Cu_2^{II}\}'] = -\left(1 + \frac{K_{d2}}{[Cu^{2+}]} + \frac{K_{d1}K_{d2}}{[Cu^{2+}]^2}\right) \Delta[(yfh1)Cu_2^{II}] \quad (S27)$$

The substitution of eq. S27 in eq. S24 leads to eq. S28:

$$\frac{d\Delta[\{(yfh1)Cu_2^{II}\}']}{dt} = -\left[k_2^{Cu^{II}} \left(1 + \frac{K_{d2}}{[Cu^{2+}]} + \frac{K_{d1}K_{d2}}{[Cu^{2+}]^2}\right)^{-1} + k_{-2}^{Cu^{II}} [H^+]\right] \Delta[\{(yfh1)Cu_2^{II}\}'] \quad (S28)$$

The reciprocal relaxation time equation associated with eq. S21 is expressed as eqs. S29 & S30

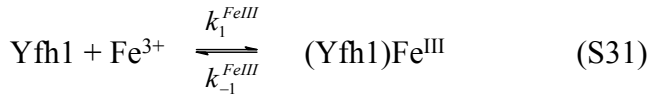
$$\tau_2^{Cu^{II}} = k_2^{Cu^{II}} \left(1 + \frac{K_{d2}}{[Cu^{2+}]} + \frac{K_{d1}K_{d2}}{[Cu^{2+}]^2}\right)^{-1} + k_{-2}^{Cu^{II}} [H^+] \quad (S29)$$

$$\frac{\tau_2^{Cu^{II}}}{[H^+]} = k_2^{Cu^{II}} \frac{[Cu^{2+}]^2}{[H^+].[Cu^{2+}]^2 + K_{d2}[Cu^{2+}] + K_{d1}K_{d2}} + k_{-2}^{Cu^{II}} \quad (S30)$$

Kinetics of Iron(III uptake)

When a solution of FeNTA is rapidly mixed with a solution of (Yfh1)₂ in Bis-Tris buffer, pH 7.0, three kinetic phenomena are observed (Figure S15). The first is a monoexponential increase in fluorescence in the 500 ms range (Figure S15A). It is followed by a second process which occurs in about 50 s as another monoexponential increase in emission (Figure S15B). The third kinetic process appears as a decrease in fluorescence and lasts about 1,000 s (Figure S15C).

The reciprocal relaxation times associated with this first phenomenon depend on Fe³⁺ concentrations. We ascribe the process to the uptake of one Fe³⁺ (eq. S30).



$$\text{With } K_1^{\text{FeIII}} = \frac{[(\text{Yfh1})\text{Fe}^{\text{III}}]}{[\text{Yfh1}][\text{Fe}^{3+}]}$$

Under our experimental conditions ($[\text{Fe}^{3+}] \gg [\text{Yfh1}]$), the reciprocal relaxation time equation associated with eq. S31 is expressed as eq. S32:

$$(\tau_1^{\text{FeIII}})^{-1} = k_3^{\text{FeIII}} ([\text{Fe}^{3+}]) + k_{-3}^{\text{FeIII}} \quad (\text{S32})$$

A good linear regression of the experimental reciprocal relaxation times against $[\text{Fe}^{3+}]$ is obtained (Figure S16). From the slope and intercept of the best line, $k_1^{\text{FeIII}} = (11.5 \pm 0.5) \times 10^4 \text{ M}^{-1} \text{ s}^{-1}$, $k_1^{\text{FeIII}} = 3.4 \pm 0.7 \text{ s}^{-1}$ and $K_1^{\text{FeIII}} = k_1^{\text{FeIII}} / k_{-1}^{\text{FeIII}} = (3.4 \pm 0.8) \times 10^4$ are determined. The K_1^{FeIII} value is, within the limits of uncertainty, identical to that determined by microcalorimetry for one iron.

The second and third kinetic processes are independent of iron and frataxin concentrations. They are, therefore, assumed to be monomolecular reaction such as a change in the conformation of the protein-metal complex ².

$$(\tau_2^{\text{FeIII}})^{-1} = (64 \pm 5) \times 10^{-3} \text{ s}^{-1}$$

$$(\tau_3^{FeIII})^{-1} = (3.3 \pm 0.2) \times 10^{-3} s^{-1}.$$

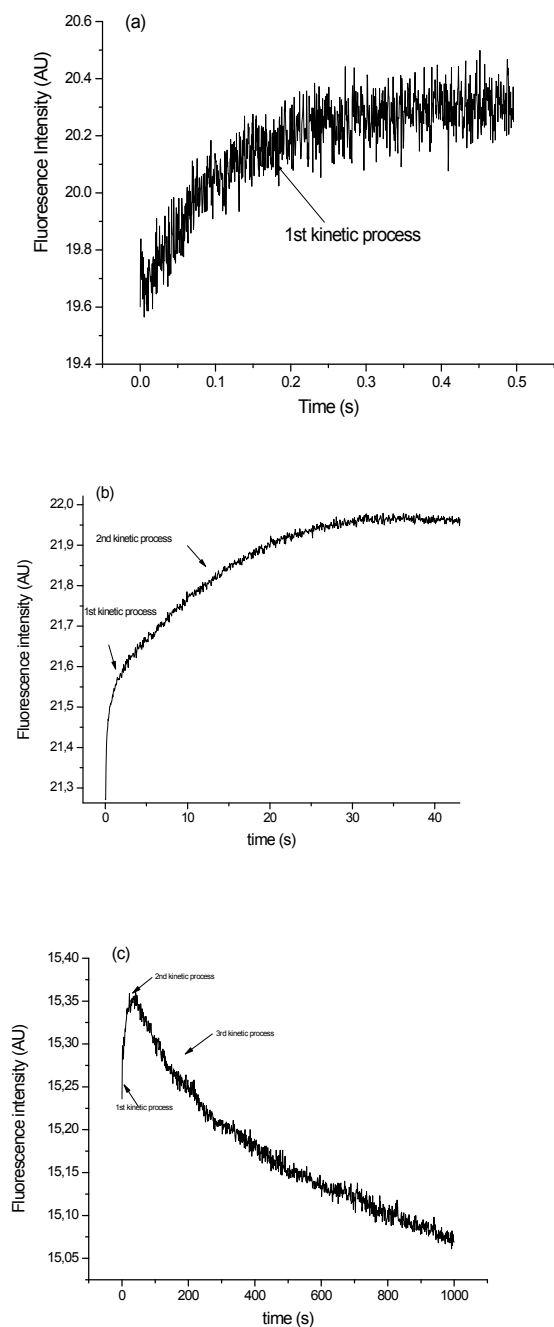


Fig. S15 Fluorescence intensity variation with time after a fast mixing of an $(Yfh1)_2$ solution ($1 \mu\text{M}$) with a FeNTA solution ($75 \mu\text{M}$) at pH 7.0, $25 \text{ }^\circ\text{C}$ and ionic strength $\mu = 0.2$ (50 mM Bis-Tris, 150 mM KCl) (a) recorded over 500 ms (b) recorded over 50 s (c) recorded over 1000 s.

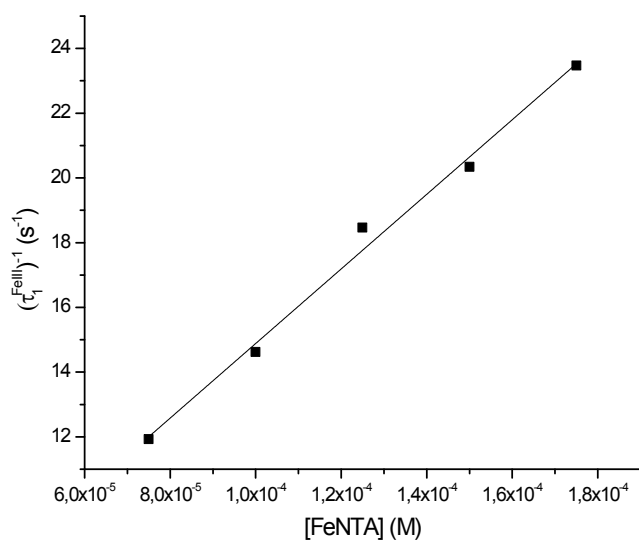


Fig S16 Plot of $(\tau_1^{FeIII})^{-1}$ against [FeNTA] at pH 7.0 with [(Yfh1)₂] = 1 μM and 75 μM ≤ [FeNTA] ≤ 175 μM; slope of $(11.5 \pm 0.6) \times 10^4 \text{ M}^{-1} \text{ s}^{-1}$; intercept, $3.4 \pm 0.7 \text{ s}^{-1}$; $r = 0.99606$.

1. C. Eid, M. Hemadi, N. T. Ha-Duong and J. M. El Hage Chahine. *Iron uptake and transfer from ceruloplasmin to transferrin*. *Biochimica et biophysica acta*. 2014; **1840**: 1771-81.
2. Z. Chikh, M. Hemadi, G. Miquel, N. T. Ha-Duong and J. M. El Hage Chahine. *Cobalt and the iron acquisition pathway: competition towards interaction with receptor 1*. *Journal of molecular biology*. 2008; **380**: 900-16.